PERGAMON

International Journal of Heat and Mass Transfer 43 (2000) 2727–2737

International Journal of HEAT and MASS TRANSFER

www.elsevier.com/locate/ijhmt

Heat transfer from a 2D backward facing step with isotropic porous floor segments

Bassam A/K Abu-Hijleh*

Mechanical Engineering Department, Jordan University of Science and Technology (JUST), P.O. Box 3030, Irbid 22110, Jordan

Received 2 March 1999; received in revised form 16 August 1999

Abstract

The incompressible laminar ($Re_H = 100$) reattaching flow over a 2D backward facing step with porous floor segments of different lengths was solved numerically using the finite element method. The focus of this study was the change in the forced convection heat transfer characteristics of the flow field due to the addition of porous floor segments. Several isotropic porous floor segment configurations with different lengths and depths were studied. The porosity of the segments was varied over a wide range by changing the value of the pressure loss coefficient ($KP = 10^{-2}$–10^{6}). The changes in the local and overall Nusselt number are reported and discussed. Depending on the configuration, axial variation of the local Nusselt number could be altered. For all configurations, the overall Nusselt number decreased by as much as 16% while the maximum local Nusselt number increased by as much as 170%, both relative to their respective values for the reference case of a solid floor.

1. Introduction

Forced convection due to fluid flow over a backward facing step has been studied extensively. Flow through porous media occurs in a wide range of engineering applications such as the flow through insulation material, grain storage, and water movement through a geothermal reservoir. Control of the heat transfer characteristics is desirable, and the control mechanism can be either active or passive. Recent work concerning active control has focused on the use of acoustic excitation [1], mass injection or bleeding [2], vortex generators [3], imposed wall heat flux [4] and moving fences or flaps [5]. Passive control methods incorporate fixed attachments to modify the flow for a given range of operating conditions. Such methods include the use of surface riblets [6], properly sized cavities [7] and porous surfaces [8]. A more thorough review of earlier work on boundary layer control can be found in the paper by Gad-el-Hak and Bushnell [9].

The current work focuses on the effect of the addition of different porous floor segments on heat transfer from a constant temperature floor of a 2D incompressible laminar boundary layer flow over a backward facing step. This model could serve as a passive control mechanism. More important, this model could be used to study the effect of fuel packing in a solid fuel combustion chamber. The solid fuel with small passages between the fuel particles could be modeled as a porous segment in an abrupt expansion type combustion chamber. The effect of each of the segment's porosity, length and depth was studied numerically. The equations were solved on a non-uniformly sized finite element mesh. The numerical method was first validated against the data of Sparrow et al. [10] for an incompressible laminar boundary layer flow over a backward

* Tel.: +962-2-295111 ext. 2640; fax: +962-2-295018.
E-mail address: bassam@just.edu.jo (B.A/K Abu-Hijleh).

0017-9310/00/$ - see front matter
PII: S0017-9310(99)00301-4

Nomenclature

D_p	normalized porous segment depth, d_p/H
d_p	depth of porous segment
H	step height
KP	pressure loss coefficient in porous region
Nu_m	maximum local Nusselt number
Nu_o	overall Nusselt number
$N(x)$	local Nusselt number
P	pressure
Re_H	Reynolds number based on mean flow velocity before step and step height
U	axial velocity
U_∞	incoming free stream axial velocity
V	transverse velocity
X	axial distance normalized by step height, x/H
X_r	normalized reattachment length, x_r/H
X_p	normalized length of porous segment
x	axial distance measured from the step corner
y	transverse distance measured from the step corner
y_{floor}	the bottom floor of the model ($y = 0$ for solid floor and $y = -D_p$ for porous section)

Greek symbols

μ	viscosity
ρ	density

facing step with constant floor temperature. The difference between the wall and the incoming free stream temperatures, $T_w - T_\infty$, was 5°C. The average free stream velocity before the step was 0.103 m/s and the step height was 22 mm. The fluid under consideration is air. The resulting Reynolds number based on the average free stream centerline velocity before the step and step height was 100. The expansion ratio, height after the step compared with height before the step, was 2.0. A schematic of the current flow field, including a porous segment, is shown in Fig. 1.

2. Mathematical model

The continuity, x-momentum, y-momentum, and energy equations for steady state, 2D and incompressible are given by [11]:

$$\frac{\partial U}{\partial x} + \frac{\partial V}{\partial y} = 0 \tag{1}$$

$$\rho U\frac{\partial U}{\partial x} + \rho V\frac{\partial U}{\partial y} = -\frac{\partial P}{\partial x} - KP\frac{\rho U^2}{2} + \mu\left[\frac{\partial^2 U}{\partial x^2} + \frac{\partial^2 U}{\partial y^2}\right] \tag{2}$$

$$\rho U\frac{\partial V}{\partial x} + \rho V\frac{\partial V}{\partial y} = -\frac{\partial P}{\partial y} - KP\frac{\rho V^2}{2} + \mu\left[\frac{\partial^2 V}{\partial x^2} + \frac{\partial^2 V}{\partial y^2}\right] \tag{3}$$

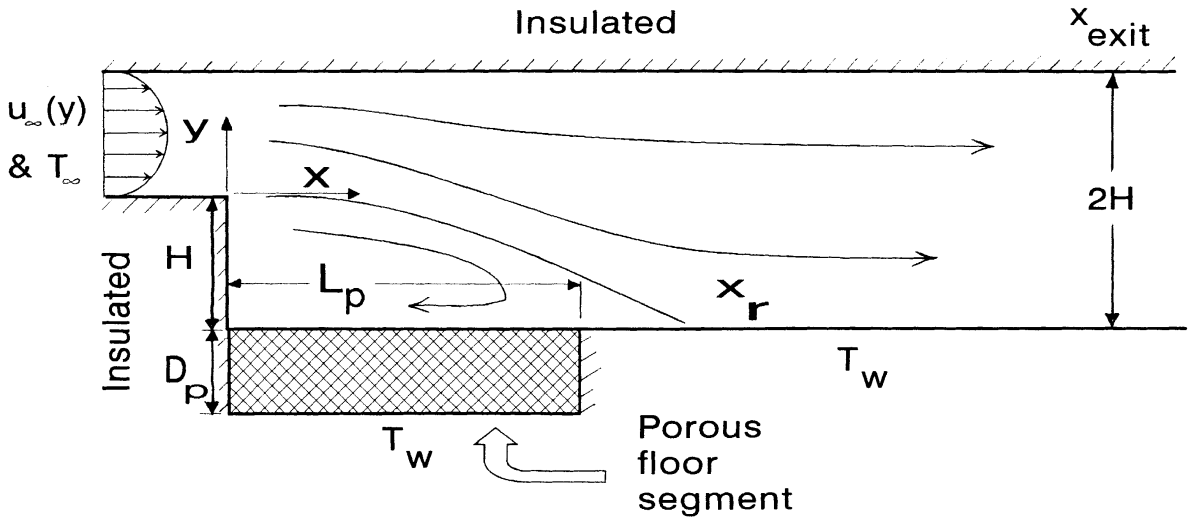

Fig. 1. Schematic of the flow.

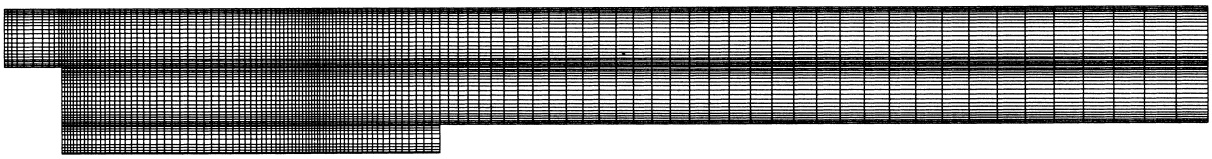

Fig. 2. Finite element mesh used for the case of $L_p = 6.6$ and $D_p = 0.5$.

$$\rho C_p\left[U\frac{\partial T}{\partial x} + V\frac{\partial T}{\partial y}\right] = k\left[\frac{\partial^2 T}{\partial x^2} + \frac{\partial^2 T}{\partial y^2}\right] \tag{4}$$

The second term on the right-hand side of the momentum equations (2) and (3) represents the extra pressure drop due to the fluid flow through the passages of the porous segment. The pressure loss coefficient factor KP is used to relate the extra pressure drop to the local velocity. There is no extra pressure loss in the non-porous part of the flow, i.e. $KP = 0$. The value of KP for different porous materials and arrangements can be found in fluid resistance handbooks such as the Handbook of Hydraulic Resistance by Idelchik [12]. The same KP value is used in both momentum equations. This models an isotropic porous material where the value of the pressure drop coefficient in both directions is the same. The local and overall Nusselt numbers based on step height (H), $Nu(x)$ and Nu_o, respectively, are given by:

$$Nu(x) = \frac{-H\frac{\partial T(x,\,y)}{\partial y}|_{y=\text{floor}}}{(T_w - T_\infty)} \tag{5}$$

$$Nu_o = \frac{1}{x_{exit}}\int_0^{x_{exit}} Nu(x)\,dx \tag{6}$$

The flow field was solved by discretizing Eqs. (1)–(4) over a non-uniform quadrilateral finite element mesh. Smaller elements were located near the walls and in regions of high gradients, i.e. at the corner of the step and close to the reattachment location. The mesh size was varied to obtain a mesh independent solution. The

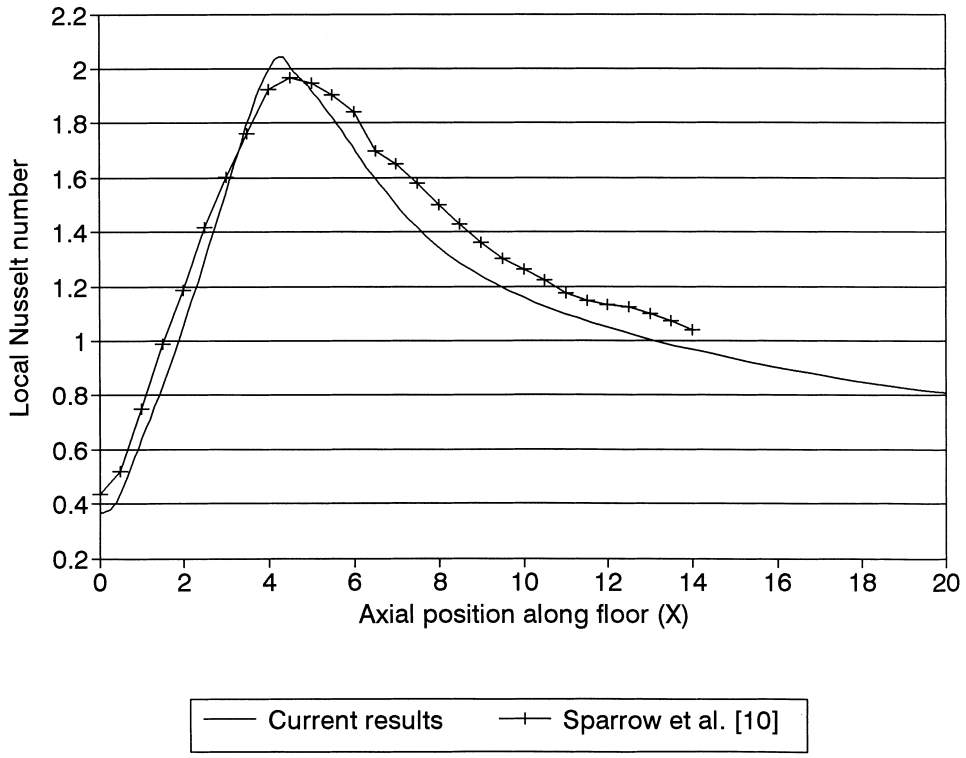

Fig. 3. Comparison between the axial variation of the local Nusselt number for the solid wall case.

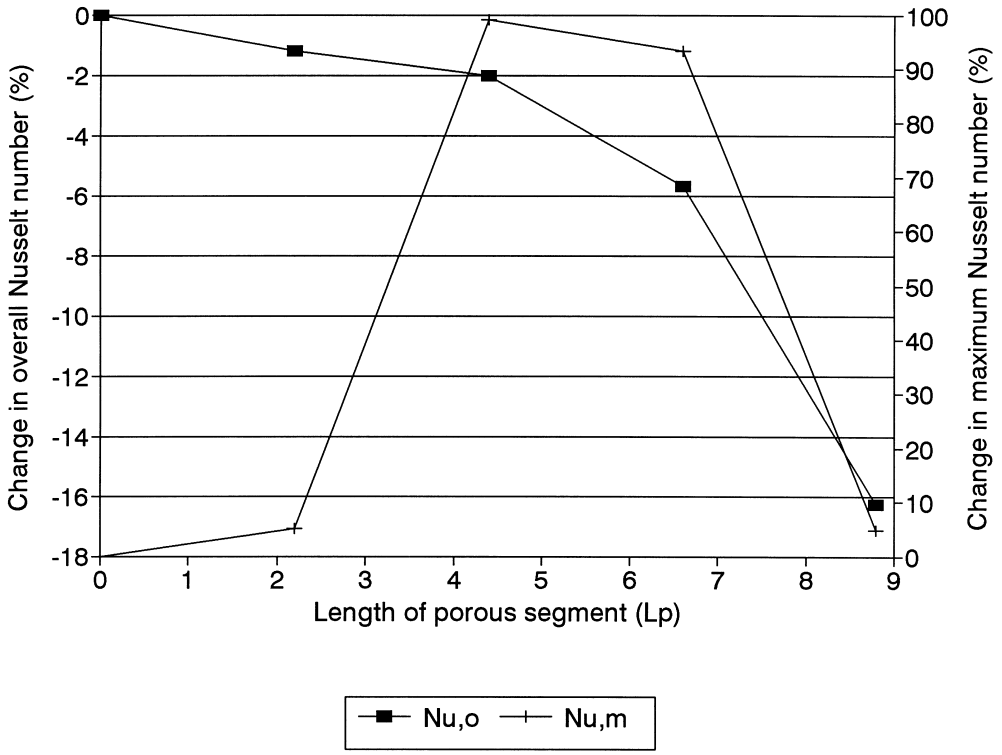

Fig. 4. Percent change in the overall and maximum Nusselt numbers as a function of the porous segment length.

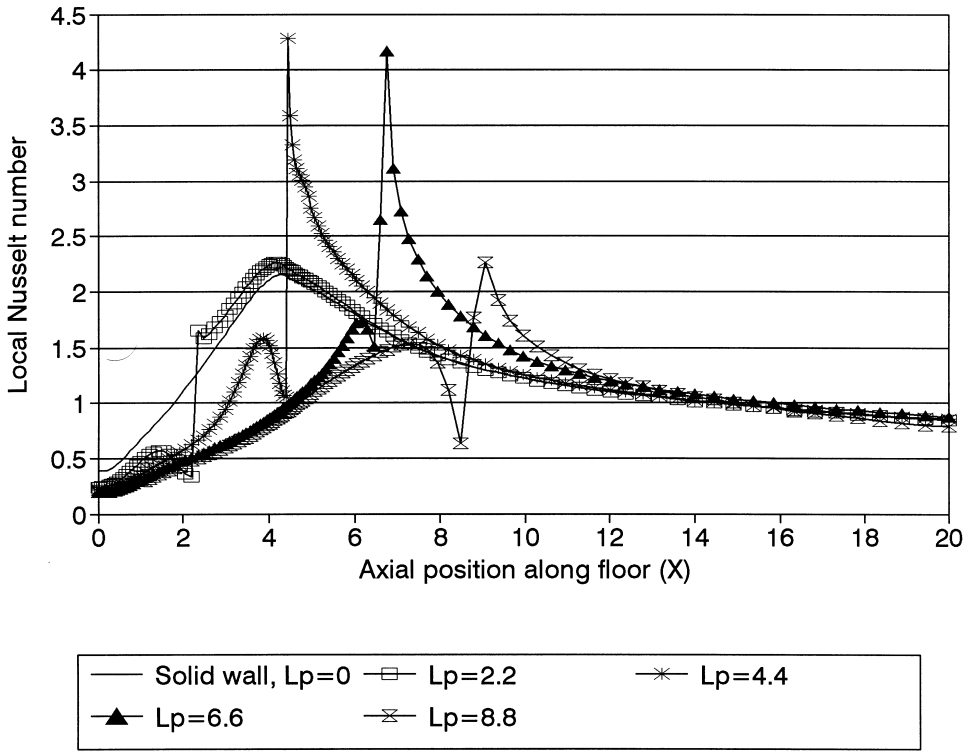

Fig. 5. Axial variation of the local Nusselt number at different lengths of the porous segments.

mesh used for the flow field, excluding the porous region, was made of 4680 elements. When the reference flow field was solved using a mesh made of 5800 elements, the change in reattachment length, values of overall and maximum Nusselt number, and location of the maximum local Nusselt number were all less than 1%. Thus, the solution obtained by using a mesh made from 4680 elements was considered mesh independent. Full mass balance between the inlet and exit planes was also achieved using the 4680 elements mesh. This is another indication that this mesh is adequate for the flow field under investigation. The placement of the exit plane was another important issue. The exit plane should be placed far enough downstream in order not to affect the computational results [13], yet not too far in order to reduce the mesh size and consequently computer memory and run time requirements. Several exit plane locations were tested, $X_{exit} = 15$–$40H$. There was minimal change in the results when the exit plane was located more than 20 step heights from the step. Thus, the exit plane was located at $20H$ for the current study. The addition of the porous segments required additional elements to discretize the porous region. The number of additional elements ranged from 250 to 3750 elements, depending on the length and depth of the porous segment under study. Fig. 2 shows the mesh for the case of $L_p = 6.6$ and $D_p = 0.5$.

The discretized equations were solved iteratively using the streamline upwind method [11]. At the flow inlet plane, velocity and temperature were specified as given by Sparrow et al. [10]. Only one boundary condition was required for the pressure. For the case of an incompressible flow, a reference value for the pressure was needed anywhere within the flow field. A pressure value of zero gage was specified at the exit

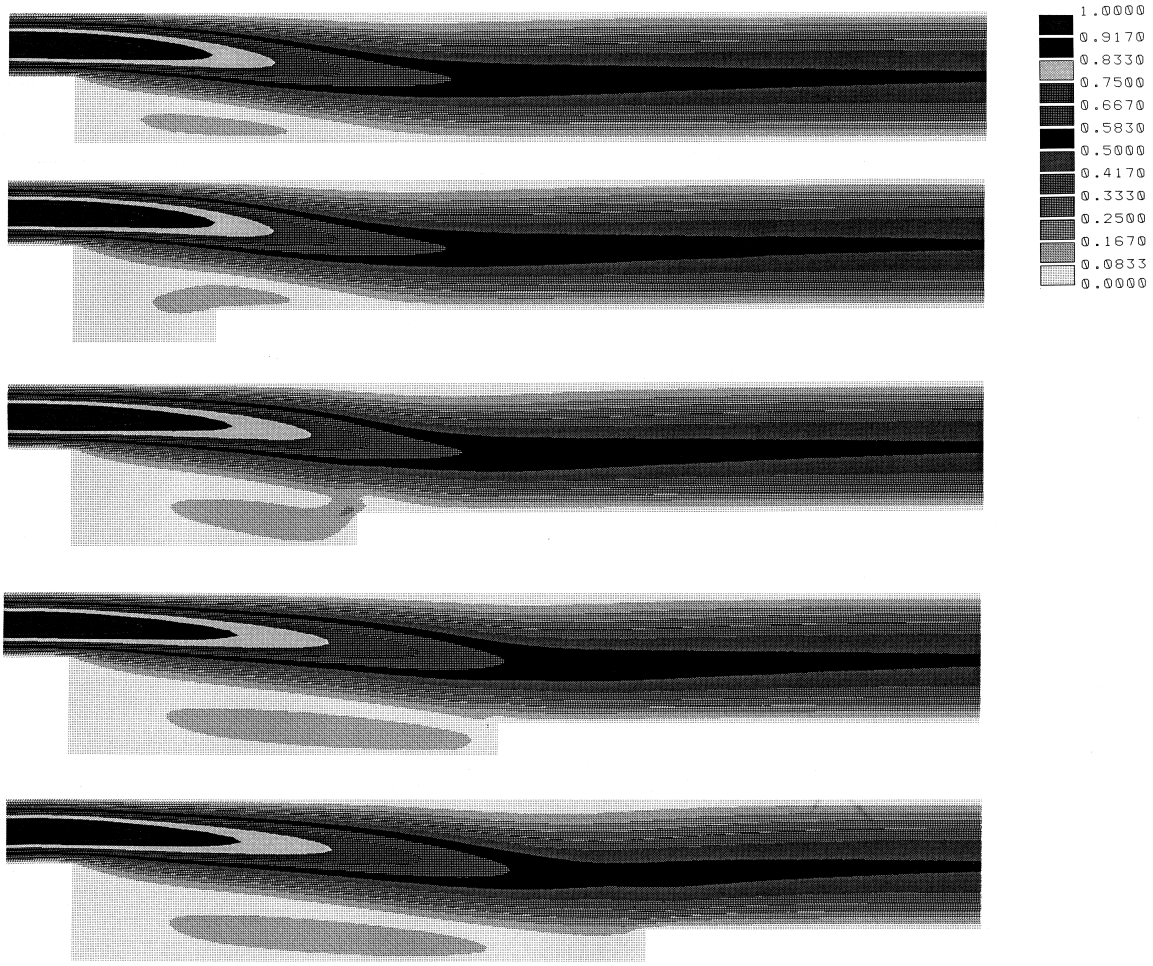

Fig. 6. Velocity contours for porous segments of different lengths. From top: reference flow, $L_p = 2.2H$, $L_p = 4.4H$, $L_p = 6.6H$ and $L_p = 8.8H$.

plane. The axial velocity and temperature gradients were set to zero at the exit plane. This served as the second axial boundary condition for the rest of the variables. The no slip condition at the walls was used for the transverse direction velocity boundary conditions. All surfaces were considered to be insulated, zero heat flux, except for the floor of the model where a constant temperature condition was specified. The solution was deemed to have converged when the residual of each of U, V, P, and T became less than 1×10^{-7}. The use of smaller tolerance values did not result in any noticeable change in the results.

The first task was to check the code's ability to predict the reference flow field as reported by Sparrow et al. [10], i.e. a solid floor. The predicted reattachment length of 4.40 step heights is in excellent agreement with the value of 4.405 step heights reported by Sparrow et al. [10]. The difference between the predicted and reported location of maximum local Nusselt number, $4.35H$ and $4.53H$, respectively, was about 4%. The fact that the maximum local Nusselt number occurs at a different axial distance from that of the point of shear layer reattachment was reported by Kondoh et al. [14]. The difference between the predicted and reported value of the maximum local Nusselt number, 2.05 and 1.95, respectively, was about 5%. Fig. 3 shows a comparison between the predicted and reported axial variation of the value of the local Nusselt numbers. The results of Sparrow et al. [10] were based on the finite difference method but little was mentioned regarding the grid used or the accuracy of the model. Sparrow's data shown in Fig. 3 were read from the figure reported in the paper [10]. Thus, some error in reading the data is inevitable. The current model has been well tested on several standard, textbook cases, flow fields with very good results. The effect of the addition of the porous segments reported herein will be discussed in terms of the percent change relative to the reference flow field as predicted by the code. Thus, the differences between the results of Sparrow et al. [10] and the current numerical results were not expected to change the conclusions of this study. The values of the maximum local and overall Nusselt numbers for the reference flow used to compare with were $Nu_m = 2.05$ and $Nu_o = 1.17$, as predicted by the current study. The changes in the local and overall Nusselt numbers were studied as a function of the following three parameters, porous segment length (L_p), pressure loss coefficient (KP) and porous segment depth (D_p). The values of two parameters were fixed at

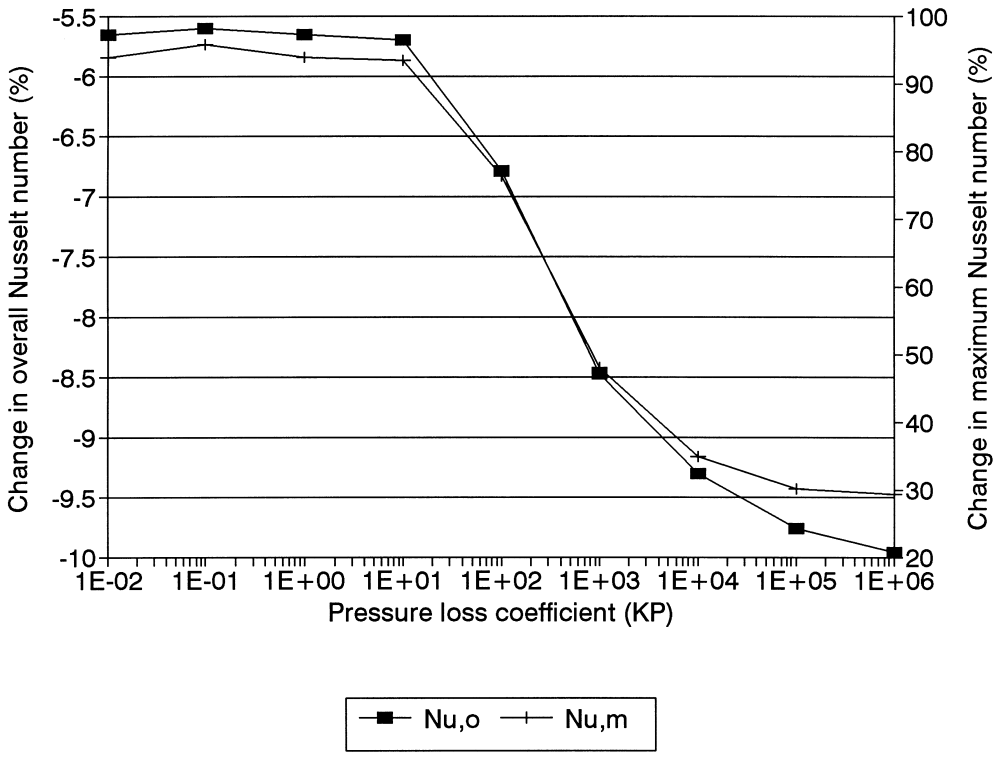

Fig. 7. Percent change in the overall and maximum Nusselt numbers as a function of the pressure loss coefficient of the porous segment.

a reference value while the third was being investigated. The reference values used were: $L_p = 6.6$, $KP = 10$ and $D_p = 0.5$.

3. Discussion

Fig. 4 shows the percent change in the local and overall Nusselt numbers at different lengths of the porous segments (L_p). $L_p = 0$ represents the solid floor case. The effect of adding a porous segment was to reduce the overall Nusselt number. The decline in the overall Nusselt number increased with L_p. The rate of decline increased for $L_p > 4.4$, $X = 4.4$ being the reattachment location of the solid floor case. Fig. 5 gives an insight into this behavior. The addition of a porous segment disturbed the region before and around reattachment but had little effect on the downstream vari-

Fig. 8. Velocity contours for porous segments with different pressure loss coefficients. From top: reference flow, $KP = 10^{-2}$, $KP = 1.0$, $KP = 10^2$ and $KP = 10^4$.

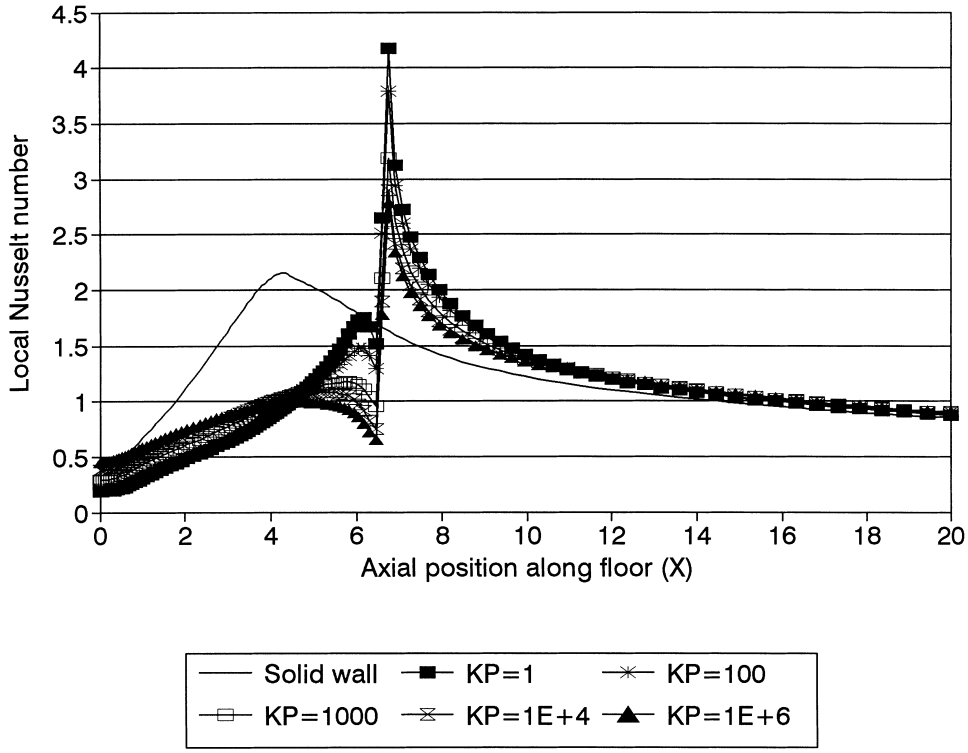

Fig. 9. Axial variation of the local Nusselt number at different values of pressure loss coefficient.

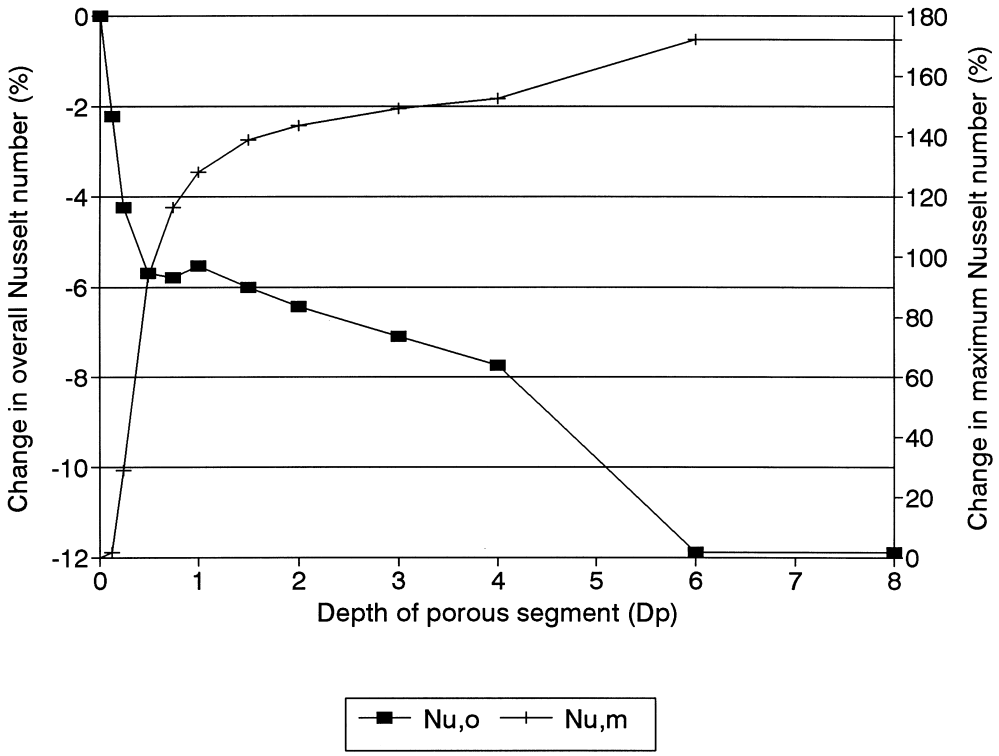

Fig. 10. Percent change in the overall and maximum Nusselt numbers as a function of the porous segment depth.

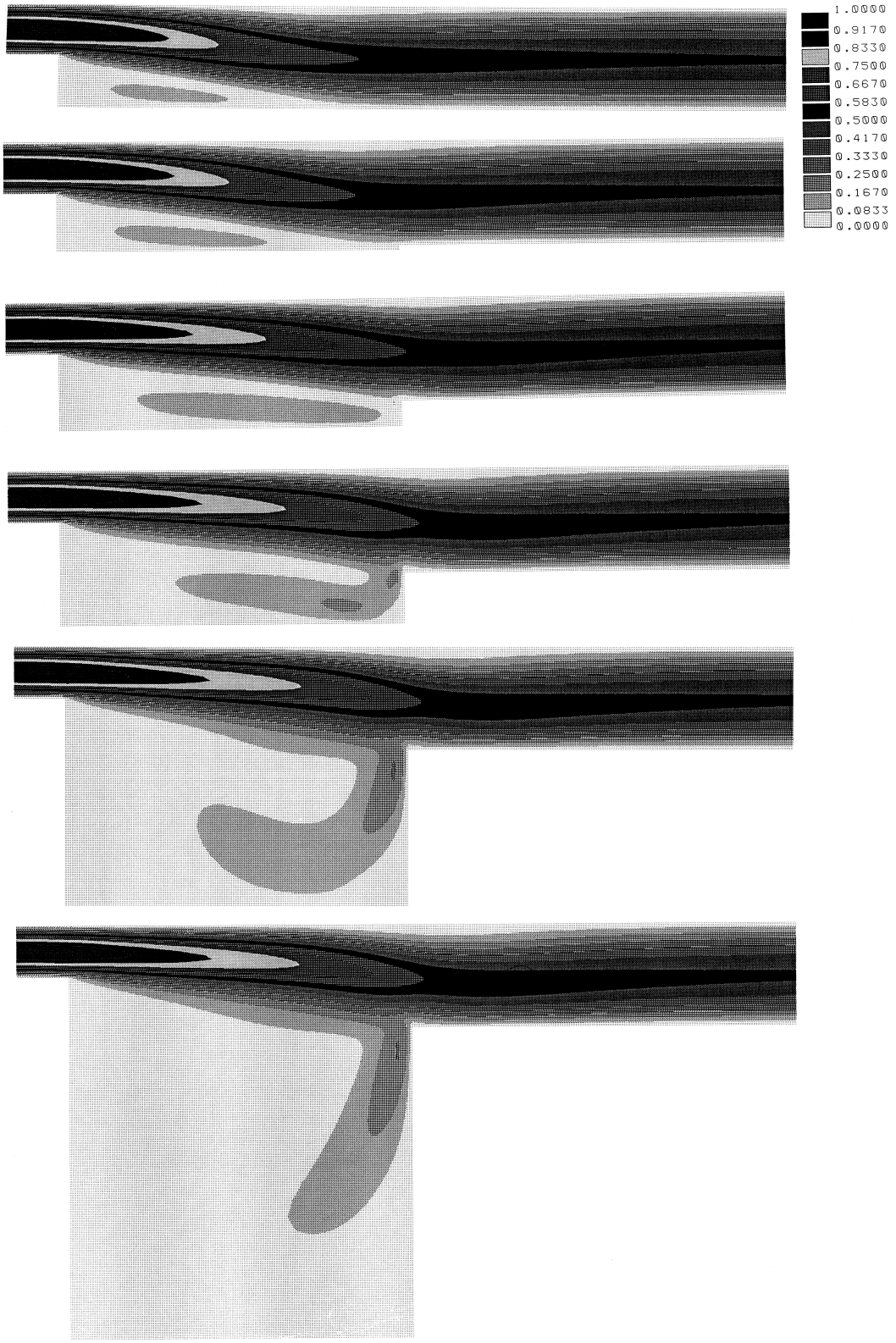

Fig. 11. Velocity contours for different depths of the porous segments. From top: reference flow, $D_p = 0.125H$, $D_p = 0.5H$, $D_p = 1.0H$, $D_p = 3.0H$ and $D_p = 6.0H$.

ation of the local Nusselt number. In the solid floor case, the local Nusselt number peaked around the reattachment location. The addition of porous segments diffused the fluid flow velocity in the recirculation region and around reattachment resulting in a substantial reduction in the local Nusselt number in these regions. The result was a reduction in the overall Nusselt number. A new boundary layer developed on the floor after the end of the porous segment and resulted in high local values of Nusselt number. Fig. 6 shows the velocity contours for the different cases of porous floor segment length. Still, these high values of local Nusselt numbers were not enough to compensate for the reduction caused by the porous region. Thus, the use of porous segments could prove useful when a high rate of local heat transfer is required. Fig. 4 shows that a high rate of local Nusselt number can only be achieved if the length of the porous segment is equal to or moderately higher than the reattachment length.

Fig. 7 shows the percentage change in the overall and maximum Nusselt number for different values of pressure loss coefficient (KP). The effect of the porous segment started at the lowest KP value of 0.01 and remained constant up to $KP = 10$. For $KP > 10$, the values of both the overall and maximum Nusselt numbers decreased with increasing KP values and tended to level off for $KP > 10^5$. This reduction can be attributed to the reduction in the fluid velocity in the porous segment and resulting reduction in the convective heat transfer. At very high values of pressure loss coefficient, $KP > 10^5$, the porous segment behaves like a solid wall and the only mode of heat transfer is conduction through the porous segment. The velocity contours confirmed the small flow through the porous segment at such high values of KP (Fig. 8). Fig. 9 shows the small change in the axial variation of local Nusselt number for $KP \geq 10^4$.

Fig. 10 shows the percent change in the overall and maximum Nusselt number at different porous segment depths (D_p). Even a shallow porous segment, $D_p = 0.125$, resulted in a noticeable reduction in the value of the overall Nusselt number and noticeable increase in the maximum Nusselt number. The increase in the maximum Nusselt number became significant for $D_p > 0.125$ and tended to level off for $D_p > 4$. For $D_p > 4$, two counter rotating recirculation regions developed in the porous segment. The lower recirculation region, bottom left side, effectively formed a virtual semi-insulated floor above the actual floor of the porous segment. Further increases in the depth of the

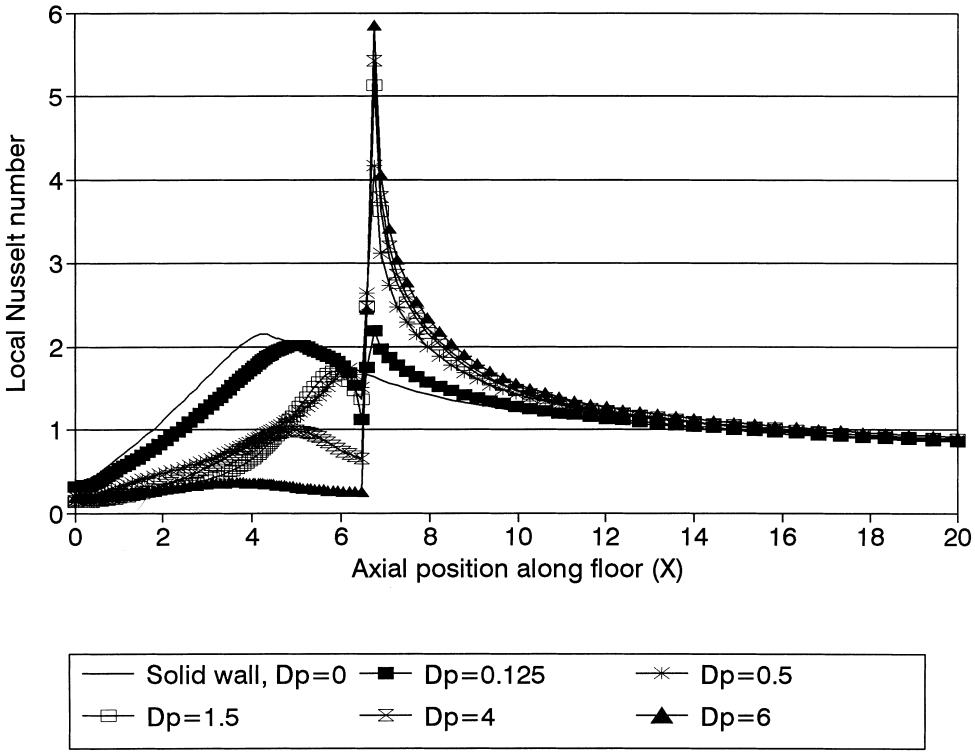

Fig. 12. variation of the local Nusselt number at different depth porous segments.

porous segment beyond $6H$ resulted in minimal effect on the fluid behavior in the porous segment (Fig. 11). This can also be seen by looking at the axial variation of the local Nusselt number for the case of $D_p = 6$ and comparing it with smaller D_ps (Fig. 12).

4. Conclusions

The addition of a porous segment as part of the floor of backward facing step configuration can be used to change the values of the overall and maximum local Nusselt numbers as well as modify the axial distribution of the local Nusselt number. Regions of high, small, or constant local Nusselt number can be attained by the proper choice of porous segment length, porosity, and depth. For all cases, the addition of a porous segment resulted in a reduction in the overall Nusselt number and an increase in the maximum Nusselt number compared to the case of a solid floor.

References

[1] R.D. Joslin, R.A. Nicolaides, G. Erlebacher, M.Y. Hussaini, M.D. Gunzburger, Active control of boundary-layer instabilities: use of sensors and spectral controller, AIAA Journal 33 (1995) 1521–1523.
[2] W.J. Chyu, M.J. Rimlinger, T.I.-P. Shih, Control of shock-wave/boundary-layer interactions by bleed, AIAA Journal 33 (1995) 1239–1247.
[3] J.W. Barter, D.S. Dolling, Reduction of fluctuating pressure loads in shock/boundary-layer interaction using vortex generators, AIAA Journal 33 (1995) 1842–1849.
[4] L.D. Karl, H.F. Fasel, Direct numerical simulation of passive control of three-dimensional phenomena in boundary-layer transition using wall heating, Journal of Fluid Mechanics 264 (1994) 213–254.
[5] I. Garsul, S. Srinivas, G. Batta, Active control of vortex breakdown over a delta wing, AIAA Journal 33 (1995) 1743–1745.
[6] P.R. Viswanabh, R. Mukund, Turbulent drag reduction using riblets on a supercritical airfoil at transonic speeds, AIAA Journal 33 (1995) 945–947.
[7] X. Zhang, Compressible cavity flow oscillation due to shear layer instability and pressure feedback, AIAA Journal 33 (1995) 1404–1411.
[8] K. Vafai, P.C. Huang, Analysis of heat transfer regulation and modification employing intermittently emplaced porous cavities, Journal of Heat Transfer 116 (1994) 604–613.
[9] M. Gad-el-Hak, D.M. Bushnell, Separation control: review, Journal of Fluids Engineering 113 (1991) 5–30.
[10] E.M. Sparrow, S.S. Kang, W. Chuck, Relation between the points of flow reattachment and maximum heat transfer for regions of flow separation, Int J. Heat Mass Transfer 30 (1987) 1237–1246.
[11] J.D. Anderson, Computational Fluid Dynamics: The Basics with Applications, McGraw-Hill, New York, 1995.
[12] I.E. Idelchik, Handbook of Hydraulic Resistance, 3rd ed., CRC Press, Boca Raton, 1994.
[13] S. Thangam, C.G. Speziale, Turbulent flow past a backward-facing step: a critical evaluation of two-equation models, AIAA Journal 30 (1992) 1314–1320.
[14] T. Kondoh, Y. Nagano, T. Tsuji, Computational study of laminar heat transfer downstream of a backward-facing step, Int J. Heat Mass Transfer 36 (1993) 577–591.